ALL-DIELECTRIC METAMATERIAL FOR ELECTROMAGNETICALLY-INDUCED TRANSPARENCY IN OPTICAL REGION

PHAM THE LINH[1,2], NGUYEN THI VIET NINH[3], NGUYEN DINH QUANG[4],
TRAN TIEN LAM[5], NGUYEN VAN NGOC[1,2], BUI XUAN KHUYEN[1],
NGUYEN THI HIEN[3], VU DINH LAM[2] AND BUI SON TUNG[1,†]

[1]*Institute of Materials Science, Vietnam Academy of Science and Technology,
18 Hoang Quoc Viet, Cau Giay, Hanoi, Vietnam*

[2]*Graduate University of Science and Technology, Vietnam Academy of Science and Technology,
18 Hoang Quoc Viet, Cau Giay, Hanoi, Vietnam*

[3]*Faculty of Physics and Technology, Thai Nguyen University of Science, Thai Nguyen, Vietnam*

[4]*Department of Physics, University of Science, Vietnam National University, Hanoi, Vietnam*

[5]*Faculty of Physics, Thai Nguyen University of Education, 20 Luong Ngoc Quyen, Thai Nguyen,
Vietnam*

[†]*E-mail:* tungbs@ims.vast.ac.vn

Abstract. *Metamaterial (MM) is emerging as a promising approach to manipulate electromagnetic waves, spanning from radio frequency to the optical region. In this paper, we employ an effect called electromagnetically-induced transparency (EIT) in all-dielectric MM structures to create a narrow transparent window in opaque broadband of the optical region (580-670 nm). Using dielectric materials instead of metals can mitigate the large non-radiative ohmic loss on the metal surface. The unit-cell of MM consists of Silicon (Si) bars on Silicon dioxide (SiO_2) substrate, in which two bars are directed horizontally and one bar is directed vertically. By changing the relative position and dimension of the Si bars, the EIT effect could be achieved. The optical properties of the proposed MM are investigated numerically using the finite difference method with commercial software Computer Simulation Technology (CST). Then, characteristic parameters of MM exhibiting EIT effect (EIT-MM), including Q-factor, group delay, are calculated to evaluate the applicability of EIT-MM to sensing and light confinement.*

I. INTRODUCTION

Over the last decade, metamaterial (MM) has emerged as an outstanding field involving materials science, engineering, optics, and nanoscience. Attention to MM is attributed to its exciting physical behaviors, such as negative refraction [1], reversed Doppler effect [2], reversed Cherenkov radiation [3]. The properties of MM are determined by its resonance structure rather than constituent materials. One can design MM to achieve desired characteristics, as long as its unit cell dimensions are subwavelength to satisfied effective medium theory [4]. As a result, the application range of MM can vary according to structural dimensions, from frequency bands of MHz [5], GHz [6], THz [7] to the optical region [8].

For years, many interesting effects such as perfect absorption [9], invisibility [10] and resolution enhancement [11] are demonstrated by exploiting MM. In addition, electromagnetically-induced transparency (EIT) [12], which is originally a quantum effect, are also mimicked based on MM. By using MM, one can overcome the rigorous requirements in creating quantum EIT effects, such as high-intensity laser and cryogenic temperature. Moreover, the reported MMs could realize the EIT effect in various spectra ranging from microwave, THz, to near-infrared region [13–15], just by modifying its unit cell dimensions. Alongside the transparent property, the EIT effect also gains attraction by the extreme dispersion in this region, leading to a significant reduction of the group velocity of the incident wave. This feature offers promising applications in slow-light and non-linear devices [13]. However, almost reported MMs exhibiting EIT effect (EIT-MMs) are metallic-dielectric combinations [16]. The appearance of the metallic component, which is highly lossy in the optical region, is the notable constraint to optical applications of EIT-MMs. Therefore, the idea of all-dielectric EIT-MMs could avoid this obstacle to provide high index and low loss optical devices [17].

In this work, we propose a simple silicon-based EIT-MM in the optical region. The designed unit cell consists of two layers including silicon (Si) on the top and silicon dioxide (SiO_2) at the bottom. The structural configuration of Si layer can be decomposed as one vertical Si bar, which plays role as a bright mode, and two horizontal Si bars, which serve as a dark mode. The coupling between them will lead to the desired EIT effect in the optical region. In addition, the structural geometry of Si layer is simple, which might be feasible for the current fabrication technology. Via the numerical method, we investigate the transparent feature of proposed EIT-MM from 580 nm to 670 nm, as well as Q-factor and group delay. It could be noted that the narrow transparent region is highly sensitive to the refractive index of the surrounding environment. Therefore, our proposed EIT-MM is a potential material for not only slow-light but also sensing applications.

II. DESIGN AND SIMULATION

Unit cell of the proposed EIT-MM, which is shown in Fig. 1, consists of two layers, a three-bar Si pattern deposited on a SiO_2 substrate. The period of the unit structure is $p = 500$ nm in both x and y directions. According to investigated wavelength region from 580 to 670 nm, we chose structural parameters of EIT-MM are, in detail, $l_1 = l_2 = l_3 = 300$ nm, $w = 50$ nm for the length and width of dielectric bars, $t_m = t_d = 50$ nm for the thickness of Si and SiO_2 layers, respectively. The distance between the center of two horizontal bars is $d_1 = 50$ nm, and the distance between the vertical bar to the unit cell central axis along y-direction is $d_2 = 50$ nm. When $d_2 = 0$, the vertical
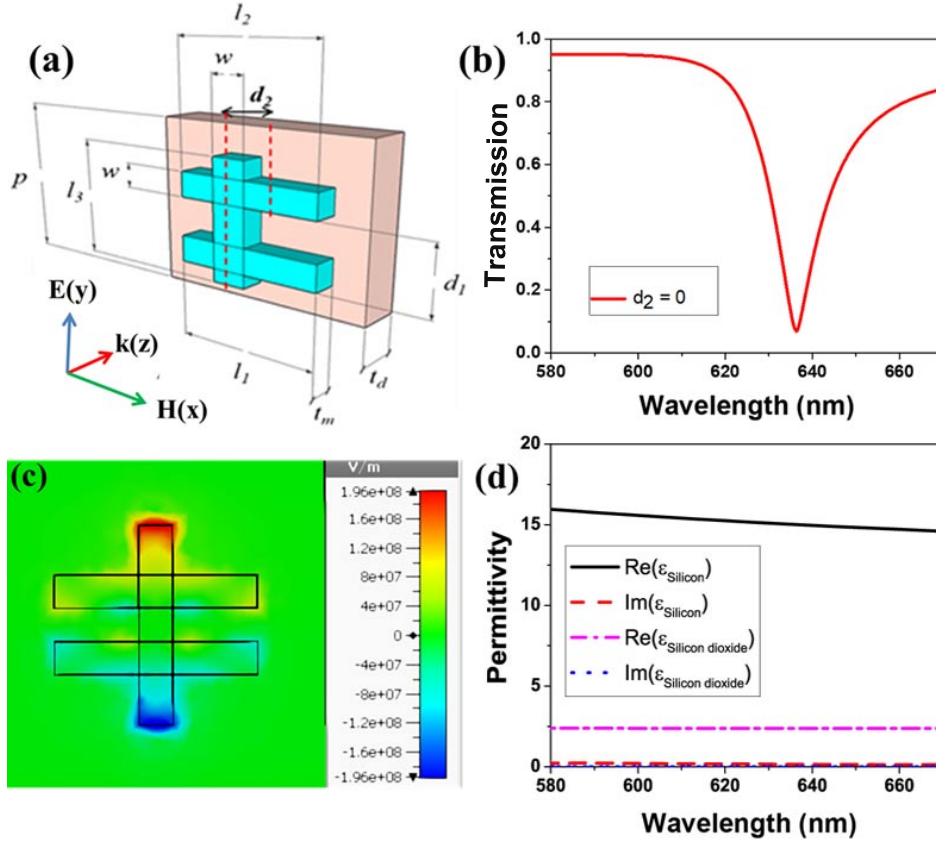
Fig. 1. (a) EIT-MM unit cell scheme, (b) transmission spectrum of symmetric EIT-MM structure, (c) distribution of electric field at transmission dip (636 nm) and (d) real and imaginary parts of permittivities of Si and SiO$_2$.

bar locates at the center of the unit cell. The dielectric parameters of Si [18] and SiO$_2$ [19] are obtained from reported experimental studies. The real and imaginary parts of permittivity values of Si and SiO$_2$ in the investigated wavelength region are shown in Fig. 1(d). In particular, the imaginary parts of permittivities are nearly 0 for both Si and SiO$_2$. The real part of Si-permittivity slightly decreases from 16 to 15 as the wavelength increases. In contrast, the real part of SiO$_2$-permittivity is nearly unchanged. This value approximately equals to 2.5 in the whole investigated wavelength range.

For simulation, we employ finite-difference frequency-domain software package CST Microwave Studio [20] to investigate the transmission properties and electromagnetic responses of the proposed metamaterial. The incident plane wave is perpendicular to the surface of MM, in which the electric and magnetic components are described as shown in Fig. 1. Two transmitters and receivers are located on the sides of the structure along the z-axis to measure transmission scattering parameters $S_{21}(\omega)$ of the incident wave when interacting with the MM medium. In

addition, we also simulate the electric field distribution of the structure to clarify the mechanism of obtained electromagnetic responses.

III. RESULTS AND DISCUSSION

In this work, we focus on analyzing transmission spectra and electromagnetic properties of all-dielectric EIT-MM when varying structural parameters. Firstly, the transmission spectrum of EIT-MM in the case of symmetric structure ($d_2 = 0$) is shown in Fig. 1(b). As can be seen from this figure, the symmetric structure provides a single-dip transmission spectrum with S_{21} is less than 0.1 at wavelength of 636 nm, regarding the fundamental resonance of this structure. We also investigate electric field distribution at the wavelength of 636 nm, and the result shows that the electric field allocates symmetrically with respect to the vertical axis of the EIT-MM structure [Fig. 1(c)].
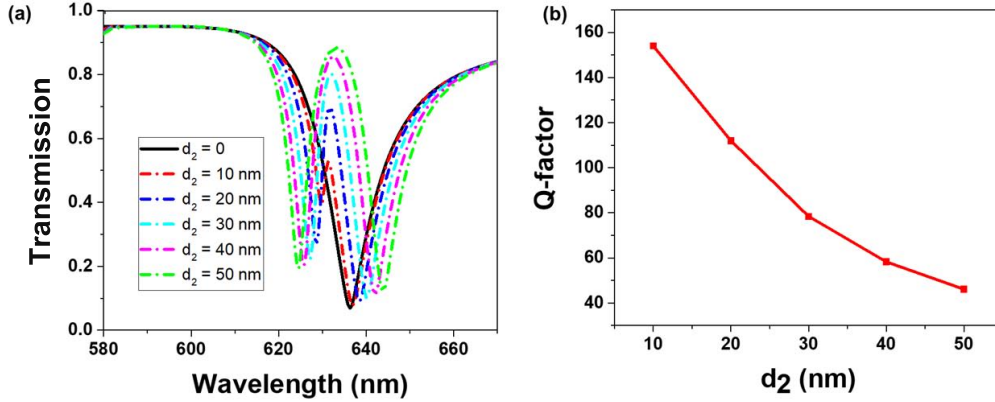
Fig. 2. (a) Simulated transmission spectra of EIT-MM structure in symmetric (solid line) and asymmetric (dashed lines) cases and (b) Q-factor of transmission peak according to values of d_2.

When the symmetry of structure is broken ($d_2 \neq 0$), the initial dip is split away and a new transmission peak appears in the same wavelength region [Fig. 2(a)]. This is also one of the distinctions of the EIT effect in MM. The transmission peak gets higher and broader as the value of d_2 increases from 10 to 50 nm. The transmission of EIT-MM reaches the highest value when $d_2 = 50$ nm. In order to assess the transmission peak of all-dielectric EIT-MM, we calculate the Q-factor of transmission peak as the following equation:

$$Q = \frac{f_0}{\Delta f},\tag{1}$$

where f_0 is the resonant frequency, Δf is given by the distance between frequency points near the peak on the spectrum, at which the intensities reach half of their maximum value. From this equation, we obtain the values of Q-factor following the variety of d_2 as shown in Fig. 2(b). Q-factor decreases as d_2 increases and the highest value of Q-factor is obtained when d_2 equals to 10 nm. However, with a higher Q-factor, the transmission undergoes lower intensity. Therefore,

we set d_2 = 30 nm to balance both properties and investigate the impact of another structural parameter.
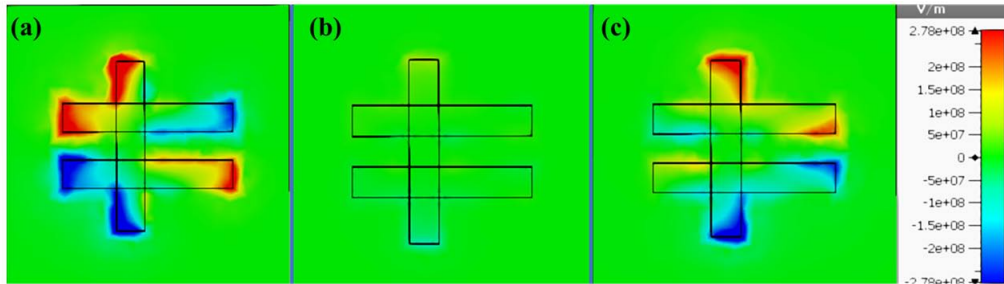
Fig. 3.   Electric field distribution in (x, y) plane at (a) first transmission-dip 627 nm, (b) transmission peak 632 nm and (c) second transmission-dip 640 nm.

To deeply understand the fundamental mechanism of the transmission peak, we investigate the distribution of electric field on the EIT-MM structure at significant wavelength positions, including both the dips and the peak (Fig. 3). At the wavelengths of two dips, the electric field strongly focuses on the left part and right part of dielectric MM structure, for shorter and longer wavelengths respectively [Figs. 3(a) and 3(c)]. Generally, in proper asymmetric-structure, the EIT effect occurs in MM through the destructive interference between two different modes at the same wavelength region. As a consequence of destructive interference, the electric field is strongly reduced at the transmission peak, as indicated in Fig. 3(b).
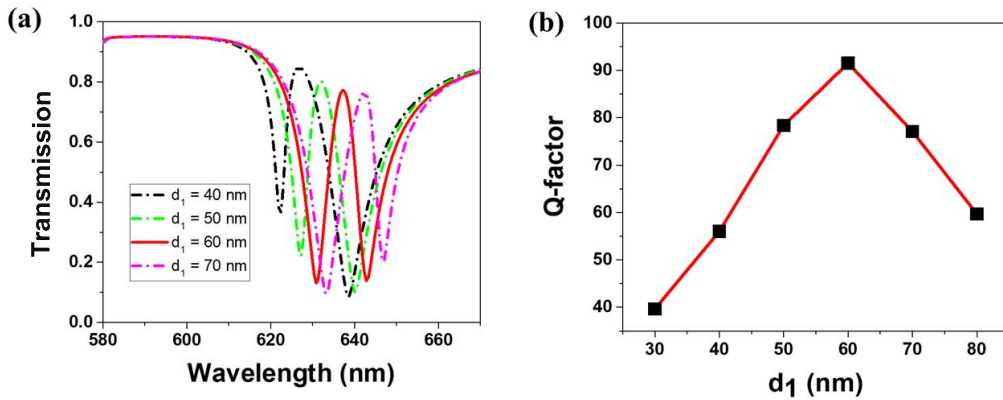
Fig. 4.   (a) Simulated transmission spectra of EIT-MM with various values of d_1 and (b) corresponding Q-factors.

Figure 4(a) shows the dependence of transmission characteristic on the gap between two horizontal bars. The increase of d_1 leads to a red-shift of resonant wavelength, and also causes a slight reduction of transmission intensity. However, our first priority, Q-factor, raises until it reaches an optimum value at a critical value of d_1 = 60 nm, then it starts to decrease [Fig. 4(b)]. Figures 5(a) and 5(b) show the transmission and transmission phase spectra of the optimized EIT-MM structure, and from this result, we finally investigate the capability of EIT-MM in slow light,
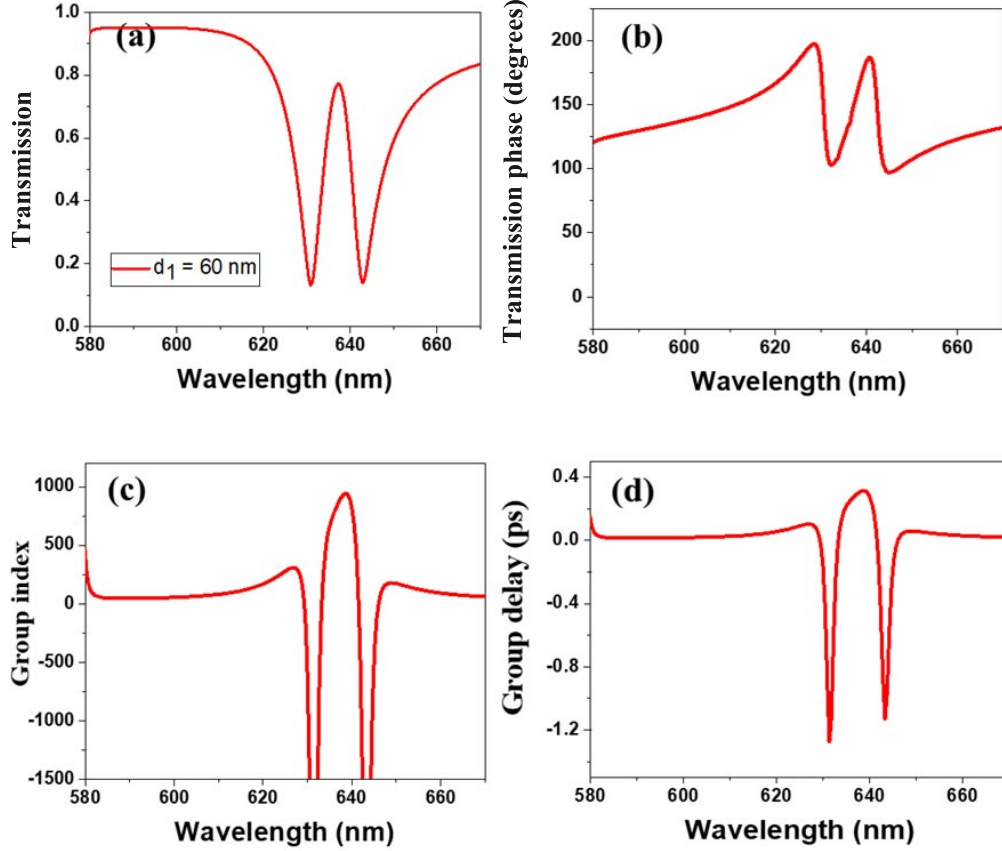
Fig. 5. (a) Transmission and (b) transmission phase spectra of optimized EIT-MM structure. Corresponding (c) group index and (d) group delay.

one of the most interesting characteristics of the EIT effect. Because the absorption and refraction properties of the medium are correlative, EIT must change the refractive index of the system when changing the absorption property [21]. The propagation velocity of the electromagnetic wave decreases with the increase of the group refractive index. A strong dispersion occurs due to the continuous steep change of phase in the transmission window, and this change reflects the speed of wave propagation. Therefore, the analog of EIT is usually accompanying by a slow-light effect [22, 23]. The group delay is used to describe the slow-light effect and is defined as [24]:

$$\tau_g = -\frac{d\varphi(\omega)}{d(\omega)} \tag{2}$$

where φ is the transmission phase shift. In addition, the corresponding group index is defined as:

$$n_g = \frac{c}{v_g} = \frac{c}{D} \times \tau_g = -\frac{c}{D} \times \frac{d\varphi(\omega)}{d(\omega)} \tag{3}$$

where c is the velocity of light in free space, v_g and τ_g are group velocity and group delay in the MM respectively, and D is the thickness of the MM. The group index of EIT-MM can reach 945 owing to strong dispersion of the transmission phase, as presented in Fig. 5(c). Meanwhile, the maximum optical delay is 0.31 ps in the transmission window, as indicated in Fig. 5(d). These values suggest that the proposed all-dielectric EIT-MM can be used for efficient slow-light applications.
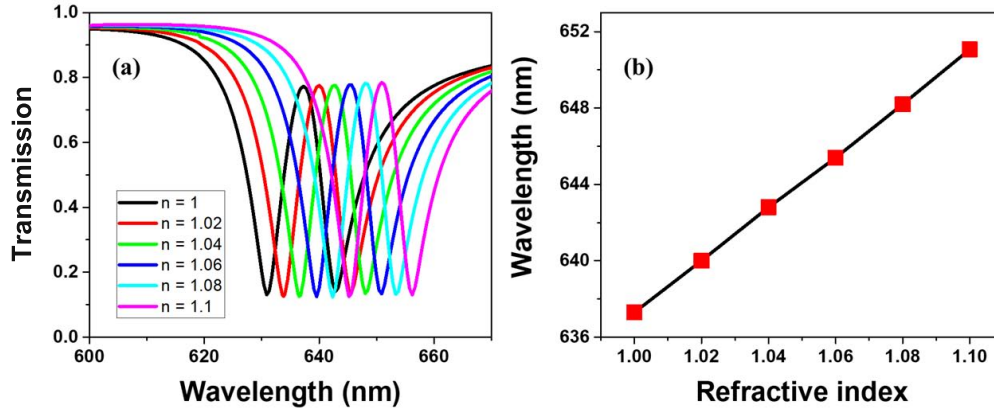
Fig. 6. (a) Simulated transmission spectra of all-dielectric EIT-MM with the refractive index of surrounding medium ranging from 1 to 1.1. (b) The transmission-peak wavelength of the structure as a function of the refractive index.

In order to apply these characteristics of EIT-MM to practical devices, we also numerically investigate the sensing capability of proposed structure. Here, we simulate the dependence of transmission spectrum on the refractive index of surrounding medium. Figure 6(a) shows the transmission spectra of EIT-MM immersed in different media with a refractive index ranging from 1 to 1.1. It is obvious that the peak position shifts towards the long wavelength as the background refractive index increases. With the small changes of media, we also realize clearly the red-shift of transmission peaks. A linear fit between the wavelength shift of the transmission peak and the background-medium refractive-index is plotted in Fig. 6(b). According to the slope of the linear fit, it is calculated that the sensitivity of EIT-MM is 135 nm/RIU. These results indicate the potential of our proposed structure in optical sensing applications.

IV. CONCLUSIONS

In this study, we propose a simple all-dielectric MM structure employing the EIT effect. Our unit cell structure comprises of two horizontal and one vertical Si bars, which is feasible to fabricate in practice. Typical characteristics of the EIT effect in MM are realized by the destructive interference between two different modes in the same wavelength region. The proposed structure is optimized by investigating structural parameters. The optimum structure shows a group index of 945, a group delay of 0.31 ps and a refractive-index sensitivity of 135 nm/RIU. The outstanding optical performance of this structure is expected to be used in a wide range of potential applications, including slow-light devices, sensors and information storage.

ACKNOWLEDGMENT

REFERENCES

[1] V. G. Veselago, *Sov. Phys. Usp.* **10** (1968) 509.

[2] S. H. Lee, C. M. Park, Y. M. Seo and C. K. Kim, *Phys. Rev. B* **81** (2010) 241102.

[3] Z. Duan, X. Tang, Z. Wang, Y. Zhang, X. Chen, M. Chen and Y. Gong, *Nat. Commun.* **8** (2017) 14901.

[4] X. Zhang and Y. Wu, *Sci. Rep.* **5** (2015) 7892.

[5] Y. Dong, W. Li, W. Cai, C. Yao, D. Ma and H. Tang, *2016 IEEE 2nd Annual Southern Power Electronics Conference (SPEC)*, 2016, pp. 1–5.

[6] B. X. Khuyen, B. S. Tung, Y. J. Kim, J. S. Hwang, K. W. Kim, J. Y. Rhee, V. D. Lam, Y. H. Kim and Y. Lee, *Sci. Rep.* **8** (2018) 11632.

[7] D. H. Tiep, B. X. Khuyen, B. S. Tung, Y. J. Kim, J. S. Hwang, V. D. Lam and Y. P. Lee, *Opt. Mater. Express* **8** (2018) 2751.

[8] J.-N. He, J.-Q. Wang, P. Ding, C.-Z. Fan, L. R. Arnaut and E.-J. Liang, *Plasmonics* **10** (2015) 1115.

[9] N. I. Landy, S. Sajuyigbe, J. J. Mock, D. R. Smith and W. J. Padilla, *Phys. Rev. Lett.* **100** (2008) 207402.

[10] E. Moghbeli, H. R. Askari and M. R. Forouzeshfard, *Opt. Laser Technol.* **108** (2018) 626 .

[11] W. Wang, N. Yadav, Z. Shen, Y. Cao, J. Liu and X. Liu, *Optik* **174** (2018) 199 .

[12] L. V. Hau, S. E. Harris, Z. Dutton and C. H. Behroozi, *Nature* **397** (1999) 594.

[13] X.-R. Jin, J. Park, H. Zheng, S. Lee, Y. Lee, J. Y. Rhee, K. W. Kim, H. S. Cheong and W. H. Jang, *Opt. Express* **19** (2011) 21652.

[14] Z. Zhao, X. Zheng, W. Peng, J. Zhang, H. Zhao and W. Shi, *Sci. Rep.* **9** (2019) 6205.

[15] D. Wu, Y. Liu, L. Yu, Z. Yu, L. Chen, R. Li, R. Ma, C. Liu, J. Zhang and H. Ye, *Sci. Rep.* **7** (2017) 45210.

[16] J. Zhang, S. Xiao, C. Jeppesen, A. Kristensen and N. A. Mortensen, *Opt. Express* **18** (2010) 17187.

[17] A. Boltasseva and H. A. Atwater, *Science* **331** (2011) 290.

[18] E. D. Palik, *Handbook of optical constants of solids*, Academic Press, San Diego, 1985.

[19] C. Tan, *J. Non-Cryst. Solids* **223** (1998) 158 .

[20] http://www.cst.com.

[21] P. Pitchappa, M. Manjappa, C. P. Ho, R. Singh, N. Singh and C. Lee, *Adv. Opt. Mater.* **4** (2016) 541.

[22] F. Zhang, X. Huang, Q. Zhao, L. Chen, Y. Wang, Q. Li, X. He, C. Li and K. Chen, *Appl. Phys. Lett.* **105** (2014) 172901.

[23] J. Gu, R. Singh, X. Liu, X. Zhang, Y. Ma, S. Zhang, S. A. Maier, Z. Tian, A. K. Azad, H.-T. Chen, A. J. Taylor, J. Han and W. Zhang, *Nat. Commun.* **3** (2012) 1151.

[24] H. Lu, X. Liu and D. Mao, *Phys. Rev. A* **85** (2012) 053803.